ACS SyntheticBiology

pubs.acs.org/synthbio Letter

A Biosensor for Detection of Indole Metabolites

Jiefei Wang,[†] Chao Zhang,[†] and W. Seth Childers*

Cite This: *ACS Synth. Biol.* 2021, 10, 1605−1614 Read Online

ACCESS | Metrics & More | Article Recommendations | Supporting Information

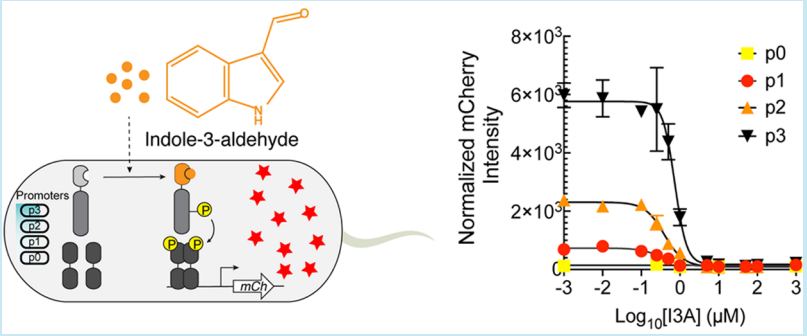

ABSTRACT: Microbially produced indole metabolites serve as a diverse family of interspecies and interkingdom signaling molecules in the context of human health, crop production, and antibiotic resistance. We mined the protein database for sensors of indole metabolites and developed a biosensor for indole-3-aldehyde (I3A). Microbially produced I3A has been associated with reducing inflammation in diseases such as ulcerative colitis by stimulating the aryl hydrocarbon receptor pathway. We engineered an *E. coli* strain embedded with a single plasmid carrying a chimeric two-component system that detects I3A. Our I3A receptor characterization confirmed binding site residues that contribute to the sensor's I3A detection range of 0.1−10 μM. This new I3A biosensor opens the door to sensing indole metabolites produced at various host−microbe interfaces and provides new parts for synthetic biology applications.

KEYWORDS: *biosensor, microbiome, indole-3-aldehyde, two-component system, Archaea, indole*

Synthetic biology has demonstrated the potential for probiotics to address a range of health issues, including the treatment of rare metabolic disorders[1] and pathogenic infections.[2,3] The lack of diverse parts to sense health-related signals limits these applications. Therefore, we mined the protein database (PDB) for sensors that could detect signals associated with gut-microbiome interactions.

Among microbiome-produced metabolites, indole and its derivatives serve as important interkingdom signaling molecules.[4] In the gastrointestinal tract, tryptophan is metabolized by three major metabolic pathways:[5] monoamine neurotransmitter serotonin (5-hydroxytryptamine, 5-HT) production,[6] nicotinic acid production through kynurenine pathway,[7] and production of indole compounds triggering aryl hydrocarbon receptor (AhR) pathway.[8] *Lactobacillus reuteri* produces indole-3-aldehyde (I3A), which is detected in gastric fluids and urine and stimulates AhR mediated transcription.[8] I3A stimulation of the AhR receptor may have broad health implications[9] that include regulating gut barrier function,[10] T cells,[11] skin inflammation,[12] central nervous system inflammation,[13] and inflammation associated with aging.[14] Similarly, pathogenic *E. coli* strains (EPEC, EHEC, and EAEC) secrete certain indole derivatives, including I3A and indole-3-acetic acid (I3AA), to kill *C. elegans*.[15] Therefore, I3A is a critical microbially produced biomarker that directly impacts health through AhR activation.

Compared to traditional detection methods, such as mass spectroscopy, cell-based biosensors take advantage of the natural ability of a cell to sense and respond to the environment. Thus, cell-based biosensors provide the potential for longitudinal measurements and noninvasive *in vivo* clinical applications.[2,16,17] Because indole compounds are mainly produced through the metabolism of tryptophan by microbes, we seek to build a sensor for indole compounds in bacteria. While indole derivatives act on eukaryotic AhR,[8,18] those interactions are nonspecific and function as a eukaryotic transcription factor, presenting challenges to repurpose the AhR as an indole bacterial biosensor. Though indole acts upon bacterial sensor BaeS, CpxA, and EvgS,[19,20] it remains unclear if those indole-receptor interactions are direct or indirect through indole's impact upon membrane potential.[21,22] Therefore, the lack of biochemically characterized

Received: March 5, 2021
Published: June 25, 2021

https://doi.org/10.1021/acssynbio.1c00090
ACS Synth. Biol. 2021, 10, 1605−1614

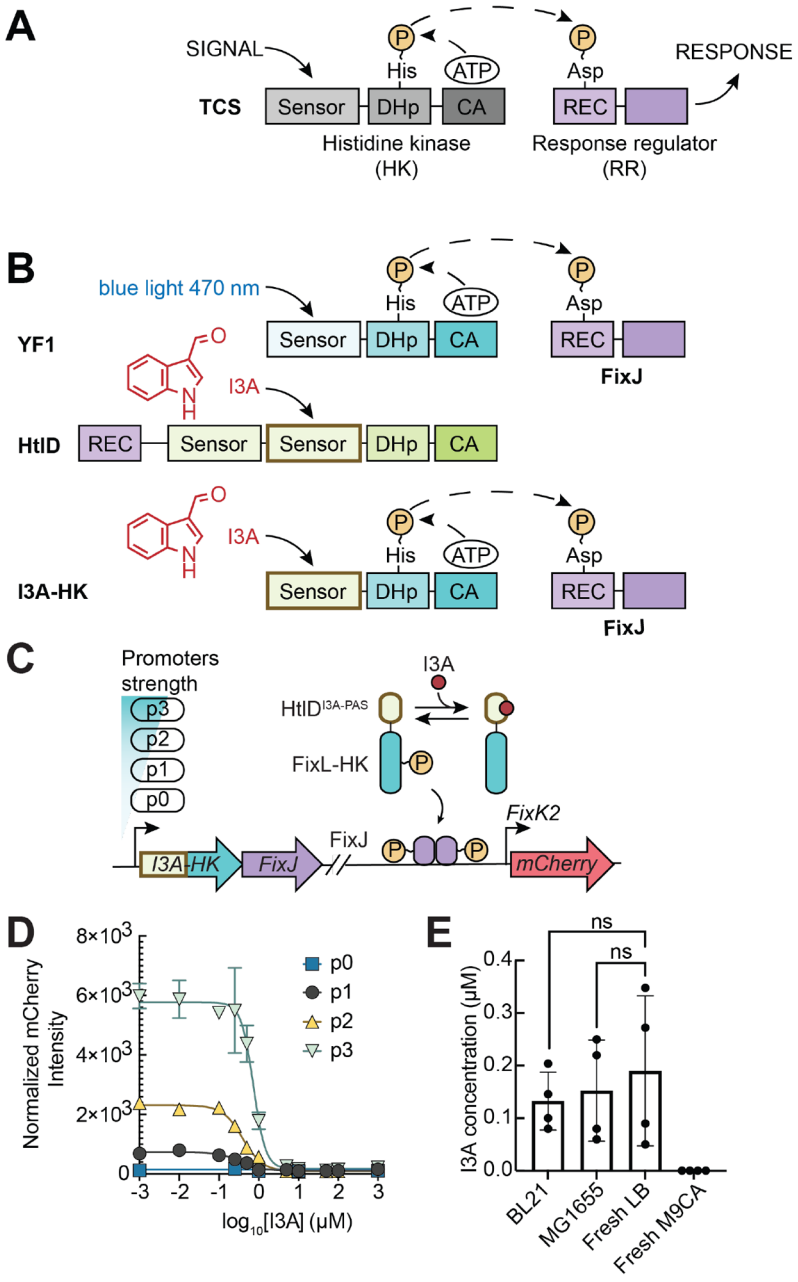

Figure 1. Design of an I3A biosensor. (A) A diagram for a typical two-component system (TCSs). A TCS is composed of a sensor histidine kinase (HK) (gray) and a response regulator (RR) (purple). A conserved HK contains a dimerization histidine phosphotransfer (DHp) domain and a C-terminal ATP-binding catalytic domain (CA) domain. The RR includes a receiver (REC) domain and a DNA binding domain. The signal regulates autophosphorylation of a conserved histidine in the DHp domain. Further phosphotransfer from the DHp domain to the REC domain results in downstream gene regulation. (B) Design of an I3A sensing chimeric histidine kinase I3A-HK. YF1 is a chimeric protein that consists of a light-sensing PAS domain and FixL-HK domain, the conserved kinase core from FixL.[55] The HtlD$^{I3A\text{-}PAS}$ domain, an I3A binding PAS domain, is the second PAS domain in the HtlD as indicated (brown box). The chemical structure of I3A is shown (red). We swapped the light-sensing domain in YF1 to the HtlD$^{I3A\text{-}PAS}$ and generated the chimeric protein I3A-HK. (C) The construct pDusk-I3A_p0-p3 for I3A-repressed *mCherry* expression. I3A regulates the activity of I3A-HK in phosphorylating the FixJ, which stimulates transcription of *mCherry* at the *FixK2* promoter. I3A repressed expression of *mCherry*. (D) I3A dose−response curve for pDusk-I3A_p0-p3. Normalized fluorescent intensity to OD_{600} was plotted against the concentration of I3A. See the curve fitting results in Table 1 for the three biological replicates. Data represent the mean ± SD of 3 biological replicates. No data point has been excluded. (E) The quantification of I3A extracted from culture media and saturated *E. coli* strains in LB media as determined by LC-MS. The I3A concentrations are plotted in the bar chart. Data represent the mean ± SD of at least 4 biological replicates. ns: not significant, $p > 0.05$ as determined by a two-sided Student's *t* test.

indole metabolite sensors prevents the use of this biomarker in health applications in bacteria.

One of the primary biochemical systems microbes use to sense their surroundings is two-component systems (TCSs). TCSs provide a cornerstone of bacterial signaling and coordinate processes such as cell cycle regulation,[23] chemotaxis,[24] cell−cell communication,[25] and bacterial virulence.[26] A TCS consists of a histidine kinase (HK) and a response regulator

https://doi.org/10.1021/acssynbio.1c00090
ACS Synth. Biol. 2021, 10, 1605−1614

Table 1. Fitting for the Dose−Response Curves[a]

media	strain	bottom	top	IC_{50}/EC_{50} (μM)	Hill slope	fold change
LB	pDawn-I3A	2959 (497)	33976 (2328)	11.5 (7.8)	0.7 (0.3)	11.8 (3.0)
LB	pDusk-I3A_p1	116 (26)	739 (128)	0.3 (0.1)	−1.8 (0.6)	6.4 (0.5)
LB	pDusk-I3A_p2	94 (11)	2325 (107)	0.4 (0.1)	−1.8 (0.4)	25.0 (4.2)
LB	pDusk-I3A_p3	168 (40)	5804 (475)	0.7 (0.1)	−2.7 (1.0)	35.5 (6.4)
M9CA	pDawn-I3A	401 (177)	9494 (2759)	3.3 (0.4)	2[b]	25.3 (5.6)
M9CA	pDusk-I3A_p3	112 (43)	2624 (718)	2.1 (0.6)	−1.5 (0.2)	24.1 (2.5)

[a]Each curve is fitted to the Hill equation with default settings in Prism9. Media: growth media. Bottom: predicted minimal normalized mCherry intensity; Top: predicted maximal normalized mCherry intensity. The mean and SD are reported in the table for three biological replicates. Standard deviation estimates are in parentheses. [b]Hill slope was fixed for the fitting.

(RR), which are responsible for sensing environmental signals and regulating cellular processes, respectively (Figure 1A). TCSs are promising targets for engineering biosensors for three reasons.[27]

First, TCSs provide a warehouse of sensors,[28] including pH, metals, quorum sensing compounds, and secondary metabolites. For instance, TCSs sensing a broad spectrum of light and have been leveraged as optogenetic tools in *E. coli*.[29−33] TCS sensing thiosulfate has been developed and applied in *E. coli* for diagnosing colon inflammation in mice.[3,34] Also, TCS metabolic sensing has been developed to screen unique chassis producing small molecules and feedstock.[34−38] Despite significant HK characterization progress, the signals that stimulate most HKs remain unknown.[39−41] The fact that signals remain unknown is partially due to the lack of crystal structures of sensors cocrystallized with their stimulating ligands.

Second, TCSs have remarkable plasticity in how signals flow within and between the HK and RR. On the one hand, the sensing domain can be swapped with homologous sensory domains to sense different signals.[42,43] On the other hand, TCSs also exert diverse outputs that include regulation of transcription, translation, motility, and proteolysis.[44−46] Additionally, the HK-RR protein−protein interaction interface can be engineered to alter phosphate transfer to other response regulators.[47] Therefore, the two-component systems' modularity allows for the straightforward and customized rewiring of a signal input to desired signaling outputs.

Third, productive cross-talk among several TCSs can function as an integrated multikinase network.[48] Multikinase networks allow sensing multiple signals simultaneously and minimize the chance of off-target regulation in a physiological environment. For example, to improve the stringency of uranium sensing, two functionally independent TCSs, UzcRS, and UrpRS, were assembled as a AND gate.[49]

Here we identified an I3A binding domain and engineered a chimeric HK that regulates mCherry expression upon the addition of I3A in *E. coli*. We engineered two one-plasmid systems, which encode the I3A binding domain within a chimeric histidine kinase and its cognate response regulator, FixJ. This initial indole metabolite sensor provides a scaffold in synthetic biology for engineering sensors for a diverse repertoire of indole metabolites. This includes metabolites such as indole, which is known to induce virulence factors, promote resistance to pathogens, and promote homeostasis of gut epithelial function.[5,8,50]

RESULTS AND DISCUSSION

Identification of an Indole-3-aldehyde Binding Sensory Domain. We mined the PDB for bacterial sensory domains that interact with signals in human microbiome environments. We focused our search upon Per-Arnt-Sim (PAS) domains, as they are essential sensing modules that commonly regulate HKs. A total of 1293 PAS domain entries were found, and 38 entries were identified that bind unique ligands (Table S1).

Among ligand-associated PAS domains, we identified a PAS domain cocrystallized with I3A (PDB: 3BWL).[51] I3A plays a vital role in maintaining mucosal homeostasis by stimulating the AhR signaling pathway.[5,8] The I3A-binding PAS domain belongs to the halobacterial transducer of rhodopsin (HTR)-like protein (HtlD, UniProt Q5V5P7)[52] encoded by *rrnAC0075* in halophilic Archaeon *Haloarcula marismortui*. Accordingly, we named the I3A binding PAS domain as $HtlD^{I3A\text{-}PAS}$ in this work and characterized the ability of $HtlD^{I3A\text{-}PAS}$ to serve as an I3A biosensor.

Engineering a Two-Component System in *E. coli* to Sense Indole-3-aldehyde. The HtlD signaling protein consists of a receiver domain (REC) followed by an HK domain (Figure 1B). However, there are no cognate RRs or histidine phosphotransfer proteins (Hpt) within the proximal genomic regions. The lack of knowledge of the downstream RR and the regulating set of genes prevented our ability to refactor the entire signaling system in *E. coli*. To overcome this problem, chimeric HKs have demonstrated the ability to exchange sensory domains for producing biosensors.[42,43] One such example is the blue light-sensing chimeric histidine kinase YF1.[43,53,54] The sensory domain of the blue light-sensing YF1 is a LOV (light-oxygen-voltage sensing) domain which is a PAS domain family member ($YF1^{(LOV)\text{-}PAS}$). This blue light sensor is also structurally similar to the $HtlD^{I3A\text{-}PAS}$ (Figure S1A). Therefore, to exploit the I3A sensing capabilities of $HtlD^{I3A\text{-}PAS}$, we swapped the LOV sensory domain from YF1 with the $HtlD^{I3A\text{-}PAS}$ and tested if the chimeric HK could sense I3A.

To determine the optimal sensor-HK chimera fusion site, we exploited a set of conserved D-(A/I/V)-(T/S)-E residues at the C-terminus of the PAS domain fold. This conserved motif forms a network of hydrogen bonds with the central beta-sheets of the PAS domain fold.[55,56] As demonstrated with the YF1 chimera construction,[55] this C-terminal motif in the PAS domain may provide a conserved modular point to swap PAS sensory domains. Therefore, we swapped the $YF1^{LOV\text{-}PAS}$ up to its DIT motif with the $HtlD^{I3A\text{-}PAS}$ up to its DIT motif and named the chimeric protein I3A-HK (Figure 1B, Figure S1B).

We introduced the chimeric *I3A-HK* gene into two plasmids, pDusk, and pDawn,[53] containing well-characterized parts downstream of the sensor. Upon signal stimulation, pDusk functions as an OFF sensor, displaying high reporter gene transcription in the dark and is transcriptionally repressed by blue light. In contrast, upon signal stimulation, pDawn is an ON sensor that exhibits low gene transcription in the dark that is

https://doi.org/10.1021/acssynbio.1c00090
ACS Synth. Biol. 2021, 10, 1605−1614

activated upon exposure to blue light.[53] We designed and constructed plasmid pDusk-I3A_p1. Within the plasmid pDusk-I3A_p1, a bicistronic operon regulated by the promoter p1 controls the constitutive expression of the *I3A-HK* gene and its cognate response regulator *fixJ*. I3A regulates phosphorylation of the FixJ RR; then, in turn, phosphor-FixJ represses transcription of the *mCherry* reporter gene[53,55] (Figure 1C). To invert the signal so that the introduction of I3A increases the reporter gene expression, we modified the pDawn plasmid[53] to incorporate the *I3A-HK* gene resulting in the plasmid pDawn-I3A (Figure S2A). In the engineered pDawn-I3A plasmid, I3A represses the expression of the λ phage repressor *cI*, which represses the expression of mCherry through the λ promoter *pR*.[53,57]

Upon addition of 10 μM I3A to strains containing the pDusk-I3A_p1 plasmid, we observed no impact upon cell growth (Figure S2B) and a 3-fold decrease in mCherry expression relative to cultures supplemented with DMSO (Figure 1D). An I3A titration yielded a dose−response curve with an IC_{50} of 0.3 ± 0.1 μM (Figure 1D, Table 1) in LB media. Similarly, upon the addition of 10 μM I3A to strains containing the pDawn-I3A_p1, we observed a 2.5-fold increase in mCherry expression (Figure S2C). Further I3A titration studies yielded a dose−response curve with an EC_{50} of 11.5 ± 7.8 μM (Figure S2C, Table 1) in LB media. Therefore, we have constructed two biosensors that repress or stimulate output gene expression upon the addition of I3A.

Tuning the Dynamic Range of the I3A Sensor. One approach to improving the dynamic range is to tune the ratio of receptor and substrate concentration.[32] To adjust the receptor to substrate ratio, we varied the promoter of *I3A-HK* using a set of well-characterized promoters from the BIOFAB kit[58] (Figure 1C, Table S2), including weak (p0), medium (p2), and strong (p3) promoters (Table S2). We grew *E. coli* cultures carrying constructed plasmids in the presence of DMSO or I3A at various concentrations to determine the effect of I3A upon the mCherry expression (Figure 1D). The dose−response curves were fitted to the Hill equation, as shown in Table 1. Replacing the promoter enlarged the dynamic range, consistent with the strength of the promoter region (Table S2), with observed fold changes of 6.4-fold for p1, 25-fold for p2, and 35.5-fold for p3. The IC_{50} is 0.4 ± 0.1 μM for p2 and 0.7 ± 0.1 μM for p3, similar to the IC_{50} for p1. The weakest selected promoter (p0) displayed no observable changes in mCherry expression upon the addition of I3A. Therefore, we demonstrated that the response to I3A could be tuned predictably by varying the promoter strength for the operon encoding *I3A-HK* and its cognate RR *fixJ*. As shown for other engineered TCS biosensors,[3] tuning HK and RR independently could be further applied to improve the I3A sensing properties.

Luria−Bertani (LB) Media Contains Residual I3A. Our ability to accurately sense I3A could be affected by the growth condition, such as endogenous production of I3A by *E. coli* or the abundance of I3A in LB media. Indeed, cocrystallization of the sensor-I3A complex indicates that I3A likely interacts with $HtlD^{I3A\text{-}PAS}$ during protein expression.[51] Moreover, past experiments suggest that *E. coli* might produce I3A.[15] To interrogate how much I3A is in the growth culture, we measured the I3A concentration in the cell culture media *via* LC-MS (Figure 1E, S3A, S3B). We observed that freshly prepared LB media contained 0.19 ± 0.07 μM of I3A, while minimal M9CA media contained no detectable amount of I3A (Figure 1E).

In comparison, we recovered 0.13 ± 0.03 μM of I3A from *E. coli* BL21 and 0.15 ± 0.05 μM of I3A from *E. coli* MG1655 wild-type strains. The I3A concentration from both BL21 and MG1655 wild-type strains is close to the amounts of I3A in fresh LB media, 0.19 ± 0.07 μM (Figure 1E). Therefore, the I3A in fresh LB media provides a 0.19 ± 0.07 μM offset to our calculated IC_{50} and EC_{50}.

To evaluate the contributions of I3A in the LB media, we compared the biosensor in DMSO *versus* supplemented with 100 μM I3A in both LB and M9CA media (Figure S3C, S3D). Notably, the mCherry expression levels in M9CA were approximately 2-fold lower than in LB media. In addition, the pDawn-I3A biosensor exhibited a 7-fold reduction in background mCherry expression in M9CA media relative to LB. We next measured the I3A dose−response curve in M9CA for pDusk_I3A_p3 (Figure S3E) and pDawn_I3A (Figure S3F). In the M9CA media, pDusk-I3A_p3 showed a higher IC_{50} (2.1 ± 0.6 μM) than in LB (0.7 ± 0.1 μM). In comparison, the pDawn-I3A system responded to I3A with a lower IC_{50} (3.3 ± 0.4 μM) in M9CA than in LB media (11.5 ± 7.8 μM). The differences in I3A-HK biosensor function in M9CA and LB are likely an additive effect of residual I3A in the LB media and global media-dependent changes in translation rates. Overall, this unexpected observation of I3A in the LB media (Figure 1E) may warrant its future investigation of I3A as a potential yeast secondary metabolite or the source of its contamination.

The PAS Binding Site and PAS Signal Transmission Motif Residues Are Required for I3A Sensing. A key question in part characterization is if structural features of the I3A chimeric sensor function as expected. Therefore, we examined the impact of I3A-HK variants that alter the I3A binding site and downstream stimulation of the HK domain (Figure 2A and 2B). PAS domains contain a conserved hinge motif D-(A/I/V)-(T/S) that couples the conformational change within the PAS domain to the conformational rearrangement that allows HK autophosphorylation.[59−61] Therefore, we mutated the DIT motif of the $HtlD^{I3A\text{-}PAS}$ to AIA (*i.e.*, D507A-T509A) to interrogate if this hinge motif was also critical for I3A sensing. We observed that the DIT to AIA mutation in the pDusk-I3A_p1 plasmid exhibited reduced mCherry expression in both DMSO and 100 μM I3A (Figure 2C). This suggests that the DIT motif variants disrupt signaling, which may be due to a lack of allostery between the sensor and HK, as observed in other HKs.[55,62,63] However, the reduced mCherry expression in DMSO for the AIA variant *versus* wild type may also result from protein misfolding or poor expression. The data indicate that the I3A stimulation of mCherry expression requires a functional PAS sensory domain.

We next tested how changes to the I3A PAS domain binding site residues impacted I3A sensing (Figure 2A and 2B). We examined three interacting residues within 5 Å of the I3A ligand: D414, D449, and F472 (PDB: 3BWL)[51] (Figure 2B). Using site-directed mutagenesis, we used pDusk-I3A_p1 as the template, mutated D414, D449, and F472 within the $HtlD^{I3A\text{-}PAS}$ individually to alanine and interrogated I3A-regulated mCherry expression (Figure 2C). To minimize mCherry expression from I3A in the LB media, we examined the I3A binding site mutants in M9CA media. Each of the I3A-HK variants displayed similar mCherry expression levels in DMSO. This suggests that the I3A-HK D414A, D449A, and F472A variants are likely folded and expressed at levels similar to the wild-type I3A-HK variant. In contrast to the wild-type I3A-HK sensor, we observed no change in mCherry expression upon the addition of 100 μM I3A (Figure

https://doi.org/10.1021/acssynbio.1c00090
ACS Synth. Biol. 2021, 10, 1605−1614

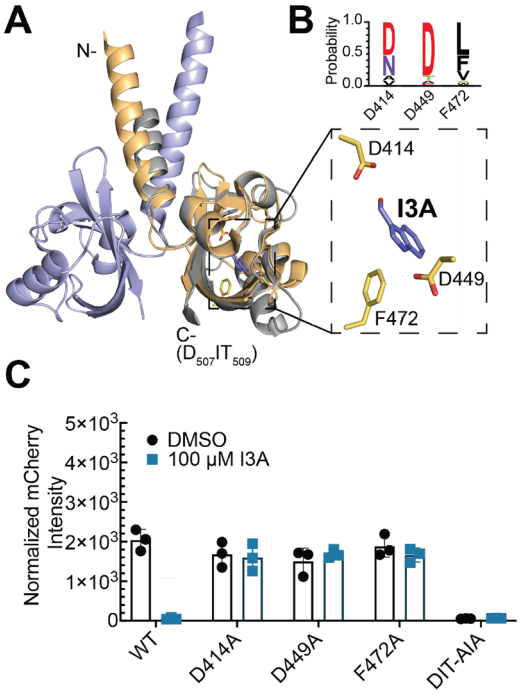

Figure 2. Interrogation of the I3A binding site. (A) Structure of the I3A binding PAS domain, $HtlD^{I3A\text{-}PAS}$ (PDB: 3BWL) deposited by Osipiuk, J., Zhou, M., Freeman, L., and Joachimiak A. at the Midwest Center for Structural Genomics.[51] Dimer of $HtlD^{I3A\text{-}PAS}$ is shown (light orange and light blue). The structure of $HtlD^{I3A\text{-}PAS}$ is aligned to the light-sensing PAS domain of YF1 (PDB: 4GCZ) (gray). The signal transmission residues are located at C- terminal in the presented structure. The residues within 5 Å to the I3A are indicated (dashed box). (B) Conservation of the potential I3A binding residues is determined by sequence alignment and plotted using WebLogo[82,83] as described in the method. (C) The response of I3A-HK variants to I3A in M9CA media. Normalized fluorescent intensity to OD_{600} was plotted with the addition of DMSO or 100 μM I3A for pDusk-I3A_p1 and its mutants. Data represent the mean ± SD of 3 biological replicates. No data point has been excluded. *$p < 0.05$ as determined by a two-sided Student's t test.

2C) for the D414A, D449A, and F472A variants. These results indicate that the selected residues, D414, D449, and F472, are critical for I3A sensing. Future engineering of the binding site residues presents opportunities to alter I3A-binding affinity and substrate specificity to other closely related indole metabolites.

Selective I3A Sensing through PAS Domain. To examine the specificity of the I3A sensing, we treated the engineered *E. coli* against a panel of 11 closely related biologically active indole metabolites at a concentration of 10 μM and 100 μM. Many of these indole metabolites only differ by one functional group where the R_1-R_4 group is substituted from −CHO in I3A to other groups (Figure 3A). Among this set, only I3A could stimulate mCherry expression at a concentration of 10 μM (Figure 3B). We observed a similar specific I3A stimulation of mCherry expression from the pDawn-I3A plasmid (Figure S4A) as from pDusk-I3A-p3 plasmid (Figure S4B). Lack of stimulation by the other closely related indole metabolites could be due to a lack of binding to the I3A sensor or the inability of the indole metabolites to cross the cell wall. At 100 μM ligand concentration, we observed a mild but statistically significant reduction of mCherry expression of less than 10% by the following: I3M, I3AA, IND, I7OH, and IMI (Figure S4B). These results indicate that I3A is a potent and specific stimulator of the I3A-HK sensor. While I3M, I3AA, IND, I7OH, and IMI weakly stimulate mCherry expression at concentrations 100-fold greater than I3A mediated stimulation of the I3A-HK sensor.

Notably, indole has been the most studied among these metabolites and reported at a much higher stimulating concentration.[21] We measured indole concentration *via* LC-MS and found *E. coli* BL21 strain produce 237.5 ± 1.1 μM indole in LB media (Figure S4C,D). However, the amount of indole endogenously produced by the *E. coli* BL21 strain expressing our chimeric I3A-HK did not stimulate complete repression of mCherry expression. Therefore, we tested higher exogenous addition of indole in the range of 500−1000 μM and observed repression of mCherry expression (Figure S4E). These data suggest that the I3A-HK has high specificity for I3A and a 100−1000-fold higher IC_{50} for indole. The indole detection could be through direct binding with the I3A sensor, or exogenous indole could stimulate biosynthesis of I3A in *E. coli*.[15] However, we also suspect that high indole concentrations used in the indole titration experiment could induce mild toxicity (Figure S4F) that impacts translation. This mild toxicity was consistent with past studies indicating toxicity at an indole concentration of 5 mM.[64] Further genetic and biochemical studies will be needed to distinguish between direct and indirect indole stimulation models.

In addition, we observed that 100−1000 μM I3AA could be detected by the I3A-HK sensor (Figure S4G) without impacting cell growth (Figure S4H). The weak indole and I3AA mediated repression of mCherry expression indicated that one should cautiously consider conditions known to produce high levels of indole or I3AA,[21] as it may provide a false-positive result for I3A detection. Critically, the mild sensing promiscuity suggests that enzyme engineering approaches upon the $HtlD^{I3A\text{-}PAS}$-like PAS domains offer the potential to alter its specificity for I3A toward other indole metabolites such as IND or I3AA.

Homologues of the Indole-3-aldehyde Binding PAS Domain. It is not clear why *Haloarcula marismortui* senses I3A and how the regulation through I3A benefits this organism. $HtlD^{I3A\text{-}PAS}$ homologues exist in archaea and bacteria (Figure S5A and Table S3), and we investigated if I3A sensing was conserved among the $HtlD^{I3A\text{-}PAS}$ homologues PAS-1 to PAS-3 (Figure 4 and Figure S5B−D). We found each homologues' response to I3A corresponds to their sequence similarity to $HtlD^{I3A\text{-}PAS}$. We observed that PAS-2-HK could repress the expression of mCherry upon the addition of I3A with an IC_{50} of 1.1 ± 0.4 μM (Figure S5E) in LB media. Similarly, expression of mCherry could be weakly repressed by the PAS-3-HK upon the addition of I3A with an IC_{50} of 0.2 ± 0.1 μM (Figure S5E) in LB media. Notably, both PAS-2-HK and PAS-3-HK exhibited a smaller dynamic range than their parent strain pDusk-I3A_p3 (Figure S5E). Critically, our validation of a direct I3A binding PAS domain that is conserved in a subset of archaea raises questions about the potential role of I3A signaling in archaea.[65]

In summary, we have developed a biosensor to detect I3A with high specificity, demonstrating the PDB provides a ripe untapped source for biosensor design. Our I3A biosensor could be applied to report on the local I3A concentration within *in vitro* imaging chambers that track bacterial biofilm formation, as done for tracking *Pseudomonas aeruginosa* on airway epithelial cells.[66] The I3A concentrations likely vary dependent upon growth conditions and the associated microbe species and hosts. However, I3A concentrations have been reported in human feces samples at 1.16 to 22.17 nmol/g.[67] While in murine

https://doi.org/10.1021/acssynbio.1c00090
ACS Synth. Biol. 2021, 10, 1605−1614

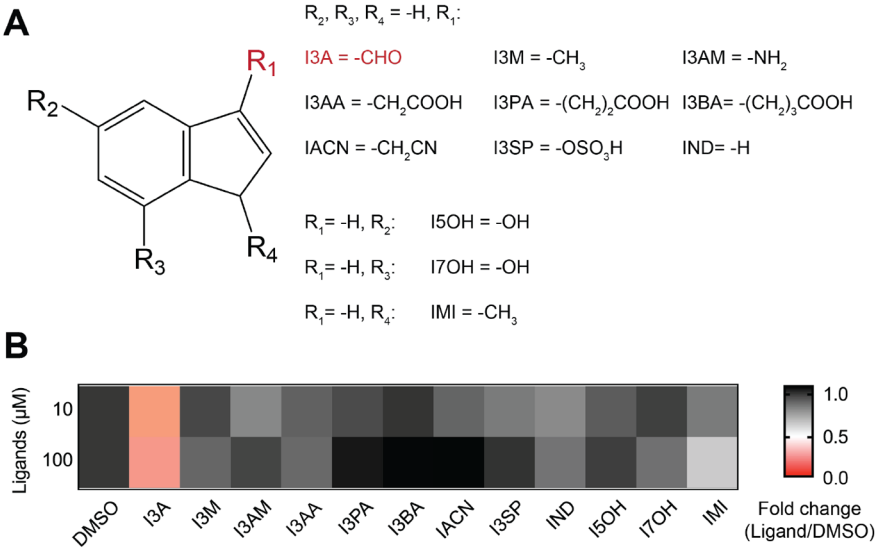

Figure 3. The selectivity of the I3A sensor. (A) Structure of indole derivatives that were used in the selectivity tests. I3A: indole-3-aldehyde, I3M: 3-methylindole, I3AM: 3-aminoindole, I3AA: Indole-3-acetic acid, I3PA: indole-3-pyruvic acid, I3BA: Indole-3-butyric acid, IACN: 3-Indoleacetonitrile, I3SP: indoxyl sulfate, IND: indole, I5OH: 5-Hydroxyindole, I7OH: 7-Hydroxyindole, IMI: 1-Methylindole (B) The selectivity of pDusk-I3A_p3 in LB media. The fold-change is reported as a ratio of normalized mCherry intensity for ligand-treated *vs* Dimethyl sulfoxide (DMSO) treated samples. The fold-change is plotted as a heat map given the gradient as shown in the figure, with a max (1.1 fold, black) and a min (0 fold, red). Data represent the mean of 3 biological replicates. No data point has been excluded. See the corresponding bar charts and the results of the test for the pDawn-I3A in Figure S3A.

samples in the range of 0.07 to 0.28 μM in C57BL/6 gastric fluids.[8] Therefore, the pDusk-I3A biosensor, with an IC50 between 0.3 and 0.7 μM, could be applied for monitoring I3A changes in murine samples. Moreover, it has been shown that indole-3-aldehyde can stimulate the aryl hydrocarbon receptors in murine Hepa1c1c7 cell lines with an EC50 of 62 μM.[68] Therefore, our I3A-HK could be applied to detect I3A at concentrations less than would stimulate the murine aryl hydrocarbon receptor pathway.

The cell-based I3A biosensor could also be applied for minimally invasive measurements of indole metabolites within the mammalian gut, as demonstrated by Daeffler *et al.* for the measurement of thiosulfate *via* a HK biosensor.[3] We also envision that this I3A biosensor could be helpful in screens to identify the I3A biosynthetic pathway in gut-associated microbes. For example, in *Lactobacillus*, an aminotransferase has been identified as crucial to produce I3A from tryptophan. However, it is unclear what other genes may be involved in I3A biosynthesis.[8]

Here we have also demonstrated that the PDB may provide a ripe untapped source for HK sensors. However, one key consideration is the protein engineering constraints upon chimeric HK biosensor design. The PAS domain family of sensors is incredibly diverse, and many may not be suitable for the regulation of an HK. PAS domains associated with HKs often utilize a PAS domain DIT motif[61] and a C-terminal α helix to induce downstream HK conformational changes upon signal sensing. Some of the earliest chimeric HK designs have demonstrated that PAS domains connected to a downstream effector domain *via* an α helix are a good candidate for chimeric-HK design.[55] However, PAS domains exhibit different mechanisms of relaying conformational change, such as local structural changes *versus* larger-scale quaternary structural changes.[69] It is less clear if PAS domains that exhibit disorder−order structural changes could regulate HK activity. Moreover, eukaryotic PAS domains may not fold properly in the bacterial cytoplasm and not be suitable for chimeric HK designs. Therefore, additional protein engineering studies will be needed to leverage other more structurally diverse PAS domains.

In summary, our I3A biosensor exhibits high specificity for I3A. However, at higher concentrations, it also senses structurally related indole and indole-3-acetic acid. Indole-3-acetic acid, a natural plant auxin, is a central plant signaling molecule regulating growth and development.[70] The interplay of auxin signaling between plants and rhizobacteria is complex.[71] For example, indole-3-acetic acid has been shown to impact nitrogen fixation and symbiosis,[72] contribute to plant growth from plant growth-promoting rhizobacteria,[73] and alter plant susceptibility to bacterial pathogens.[74] Therefore, we envision this new indole metabolite biosensor will open the door to cell-based approaches to interrogate the indole metabolites in diverse microbiome environments that include the gut microbiome and the plant-associated rhizosphere. Future enzyme engineering approaches centered upon our identified I3A binding site residues could alter specificity toward the diverse range of indole metabolites. Moreover, the I3A biosensor could be leveraged as a new part in synthetic biology applications that respond to I3A or even alter the indole signaling landscape.[75]

METHODS

Chemicals. Indole and its derivatives (Table S4) used in this work were purchased from ACROS organics and TCI America. Chemicals were stored in appropriate conditions after opening. DMSO was used to prepare a 100 mM stock solution for each ligand and frozen in a −20 °C freezer until ready to use. For dynamic range assay, 100 mM stock solution was diluted into lower concentration stocks in DMSO before adding to bacterial liquid culture.

Bacterial Strains and Growth. All *E. coli* strains, plasmids, plasmid construction methods, primers, and enzymes used in this study are listed in Table S5−S7. Primers used for the construction of plasmids were designed using j5 (Table S5).[76]

https://doi.org/10.1021/acssynbio.1c00090
ACS Synth. Biol. 2021, 10, 1605−1614

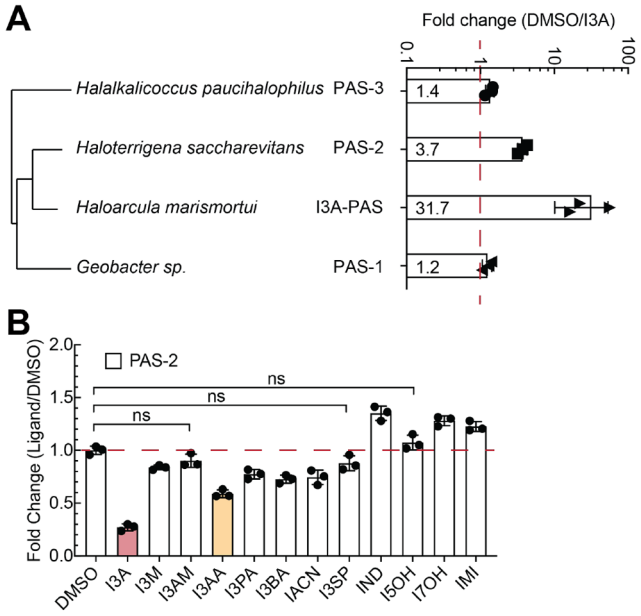

Figure 4. I3A detection is conserved among homologues of $HtlD^{I3A\text{-}PAS}$. (A) Response to I3A of the homologues of $HtlD^{I3A\text{-}PAS}$. To test the homologues, $HtlD^{I3A\text{-}PAS}$ in pDusk-I3A_p3 was swapped to each homologue and generated constructs for chimeric PAS-HKs. See the sequences of homologues in Table S3. The fold-change is reported as a ratio of normalized mCherry intensity for DMSO-treated *vs* I3A-treated samples. The red dash line indicates where the ratio equals to 1. Data represent the mean ± SD of 3 biological replicates. No data point has been excluded. The mean is indicated in a column for each homologue. See a full phylogenetic tree in Figure S5A. (B) The selectivity of PAS-2. The fold-change is reported as a ratio of normalized mCherry intensity for ligand-treated *vs* DMSO-treated samples. The red dash line indicates where the ratio equals 1. Data represent the mean ± SD of 3 biological replicates. No data point has been excluded. ns: not significant, $p > 0.05$ as determined by two-sided Student's t test, comparing ligand-treated *vs* DMSO-treated. The ligands that give a >1.5-fold change in mCherry expression are I3A (red) and I3AA (yellow). See the results for the selectivity of PAS-1 and PAS-3 in Figure S5.

All primers were purchased from Integrated DNA Technologies (IDT, Coralville, IA). All PAS domains were synthesized as gBlocks from IDT and replaced the $YF1^{LOV\text{-}PAS}$ within the pDusk plasmid (Table S5). The sequence of the chimeric site is shown in Figure S1B. For testing promoters, pDusk-I3A was used as templates and treated as p1. The 200 bp region upstream the *I3A-HK* gene in the pDusk-I3A plasmid was replaced with the selected promoter and ribosomal binding site (RBS) regions. The selected regions were cloned from BIOFAB kit strains B7, B11, and B12 for p0, p2, and p3, respectively (Drew Endy Lab, Stanford University, USA).[58] See Table S2 for sequences. All constructs above were assembled *via* Gibson Assembly using standard protocols (Table S6).[77] The plasmids pDusk-I3A and pDusk-I3A_p3 were used as templates to generate single-site mutations through the QuickChange approach. Plasmids were routinely isolated using the GeneJET Plasmid Miniprep kit (Thermofisher, USA).

E. coli strains (Table S7) were grown in LB media or on LB plates, including 1.5% w/v agar. Antibiotics were included at the following final concentrations: ampicillin, 100 μg/mL, kanamycin, 30 μg/mL or chloramphenicol, 30 μg/mL.

Fluorescence Reporter Assay. Plasmids were transformed into chemical BL21(DE3) *E. coli* cells. Cells were plated onto selective LB media plates and grown overnight at 37 °C. From a single colony, 2 mL cultures were initiated and incubated at 37 °C with shaking at 250 rpm for 12 h. The saturated cultures were normalized to $OD_{600} = 1$ and were inoculated at 1% v/v to 1 mL selected LB or M9CA media. The stock solution of ligands prepared as different concentrations in DMSO was added to the cultures at 1% v/v upon inoculation. Cultures were incubated at 37 °C with shaking at 250 rpm. After 20 h,[53] 150 μL from each culture was aliquoted into a black-bottom 96-well plate (Greiner Bio-One, USA) for fluorescence measurements, and 50 μL were aliquoted in 100 μL LB or M9CA media into a clear 96-well plate for measurements of optical density. All end point assays were measured in 96 well plates using the Infinite M1000 plate reader (Tecan, Switzerland). mCherry fluorescence was measured using an excitation wavelength of 585 nm, an emission wavelength of 610 nm, a fixed gain of 60, and a bandwidth of 5 nm. 0.02 mg/mL TAMRA SE dye (ThermoFisher, USA) was diluted and used as a standard instrumental control. The optical density was measured at 600 nm (OD_{600}). The ratio of fluorescent intensity to OD_{600} was recorded as normalized mCherry intensity. All the experiments were done with three replicates using cultures from different colonies. The mean and standard deviation of the normalized mCherry intensity were reported.

Fitting to the Hill Equation. The measure fluorescent intensity was normalized by optical density for plotting and fitting in Prism9 (GraphPad Software, San Diego, USA). The normalized mCherry intensity at each ligand concentration were fitted to the Hill equation in Prism9 with default parameters, using [inhibitor] *vs* response − variable slope function with $Y = \text{bottom} + (\text{top} - \text{bottom})/(1 + (IC_{50}/X)^{\text{hillslope}})$, or [agonist]] *vs* response − variable slope function with $Y = \text{bottom} + (X^{\text{hillslope}}) \times (\text{top} - \text{bottom})/(X^{\text{hillslope}} + EC_{50}{}^{\text{hillslope}})$. Bottom and top are minimal and maximal response, IC_{50} or EC_{50} is the concentration of ligands that gives a response halfway between top and bottom, and hillslope describes the steepness of curves.

Indole Compound Quantification by LC-MS. Quantification of indole compounds was performed using the modified method previously published.[78] Individual *E. coli* colony was picked on an LB agar plate and inoculated into a 5 mL LB culture overnight. To extract, the overnight culture was centrifuged at 4000*g* for 10 min at 4 °C, and the cell pellet and supernatant were separated. The pellet was washed with 2 mL of Milli-Q water 3 times to remove residual compounds. Then 0.5 μL Lysonase Bioprocessing Reagent (MilliPore Sigma) was added to the pellet and incubate at room temperature for 5 min. The supernatant was transferred into another 15 mL conical tube, combined with lysed cells, mixed with 5 mL of ethyl acetate (Fisher Scientific, USA), and mixed vigorously. The mixture was then allowed to stand for the layers to separate. The extraction was repeated twice, and the organic layers from each extraction were combined. The organic layer was dried with anhydrous Na_2SO_4 (Fisher Scientific, USA) and evaporated to dryness using a rotary evaporator. The crude extract was dissolved in 1 mL LC-MS grade methanol (Fisher Scientific, USA), centrifuged to remove particles, filtered with PTFE membrane (Fisher Scientific, USA), and analyzed by LC-HRMS using single ion monitoring (SIM) mode on Thermo Scientific Q-Exactive Orbitrap (ThermoFisher, USA). A gradient from 50 to 80% acetonitrile (Fisher Scientific, USA) over 30 min was used as a mobile phase using an Acclaim Polar Advantage II C18 column (Thermo Fisher Scientific, USA). For quantification of indole-3-aldehyde and indole, a standard curve that correlates the area

https://doi.org/10.1021/acssynbio.1c00090
ACS Synth. Biol. 2021, 10, 1605−1614

with the analyte concentration was used. To measure the extraction efficiency through this method, a known amount of analyte was added to water, followed by the above-described method. The efficiency is expressed as the amount calculated from the LC-MS quantification method over a known amount, which is 96.7 ± 0.7% for I3A and 97.6 ± 0.3% for IND. All biological samples were repeated three times as replicates.

Bioinformatics Analysis. The alignment of $HtlD^{I3A\text{-}PAS}$ (UniProt: Q5V5P7)[52] was performed (12/2019) using XtalPred (http://xtalpred.godziklab.org/XtalPred-cgi/xtal.pl).[79,80] The alignment was queried against the UniProtKB database with default settings (Table S8). The result was downloaded and filtered to include 40% identity and 70% coverage, resulting in 25 proteins. The sequences of the 25 proteins were downloaded from the UniProtKB database. The alignment figure was generated using Jalview (http://www.jalview.org)[81] and WebLogo (http://weblogo.threeplusone.com).[82,83]

■ ASSOCIATED CONTENT

Supporting Information

The Supporting Information is available free of charge at https://pubs.acs.org/doi/10.1021/acssynbio.1c00090.

Figure S1−S5: Structure of *HtlD*$^{I3A\text{-}PAS}$ and design of chimera I3A-HK, construction of I3A sensors, characterization of an I3A "ON" sensor, the selectivity of the I3A sensors, quantification of I3A and IND in the cell culture using LC-MS, and indole metabolite stimulation of homologues of $HtlD^{I3A\text{-}PAS}$; Tables S1−S8: PDB PAS domains with ligands, promoters used for constructs, selected homologues of $HtlD^{I3A\text{-}PAS}$, chemicals, DNA oligos used in the study, Gibson cloning strategies for plasmids, *E. coli* strains used in the study, and BLAST results for $HtlD^{I3A\text{-}PAS}$ (PDF)

Tables S1 and S8 (XLSX)

■ AUTHOR INFORMATION

Corresponding Author

W. Seth Childers − *Department of Chemistry, University of Pittsburgh, Pittsburgh, Pennsylvania 15260, United States;* orcid.org/0000-0003-1160-7767; Phone: 412-624-3058; Email: wschild@pitt.edu

Authors

Jiefei Wang − *Department of Chemistry, University of Pittsburgh, Pittsburgh, Pennsylvania 15260, United States*

Chao Zhang − *Department of Chemistry, University of Pittsburgh, Pittsburgh, Pennsylvania 15260, United States*

Complete contact information is available at: https://pubs.acs.org/10.1021/acssynbio.1c00090

Author Contributions

†J.W. and C.Z. contributed equally.

Author Contributions

W.S.C., C.Z., and J.W. conceptualized and designed the study. C.Z. and J.W. constructed plasmids and strains. C.Z. performed and collected preliminary data for I3A dose−response and ligands screening experiments on parent strains, pDawn-I3A, and pDusk-I3A_p1. J.W. performed the experiments and analyzed data. C. Z. performed and analyzed LC-MS experiments. W.S.C. and J.W. drafted the manuscript with input from C.Z. All authors provided critical feedback and helped shape the research, analysis, and manuscript.

Notes

The authors declare no competing financial interest.

■ ACKNOWLEDGMENTS

This research was funded through the University of Pittsburgh Start-up funds to W.S.C. We thank Osipiuk, J, Zhou, M., Freeman, L., Joachimiak, A., and the Midwest Center for Structural Genomics for their past work structurally characterizing the I3A sensor (PDB: 3BWL). Their tireless structural characterization efforts have created a valuable resource for the scientific community. We thank the Andreas Möglich lab at the University of Bayreuth and Addgene for providing the pDusk (Addgene Plasmid # 43795) and pDawn plasmid (Addgene Plasmid # 43796) that was used in this study. We thank the Drew Endy lab at Stanford University and Addgene for the BIOFAB promoter library (Addgene Kit #1000000037). We thank the Yiming Wang lab at the University of Pittsburgh for providing IMI and indole used in this study and Yidong Wang's generous help with bacterial cell lysate extract. We thank Xiaole Yang of the Childers laboratory for her guidance on HPLC and Dr. Bhaskar Godogu from the mass spectrometry facility at the University of Pittsburgh for providing advice on LC-MS in this study. We thank the Alex Deiters lab at the University of Pittsburgh for sharing the Tecan 100 plate reader that supported measurements in this study. We thank Dylan T. Tomares of the Childers laboratory for his comments on the figures.

■ ABBREVIATIONS

5-HT, 5-hydroxytryptamine; AhR, aryl hydrocarbon receptor; CA, catalytic domain; CNS, central nervous system; DHp, dimerization histidine phosphotransfer; DMSO, DMSO (biological grade); Hpt, histidine phosphotransfer protein; HK, histidine kinase; HtlD, HTR-like protein D; HTR, halobacterial transducer of rhodopsin; I3A, indole-3-aldehyde; I3AA, indole-3-acetic acid; I3AM, 3-aminoindole; I3BA, indole-3-butyric acid; I3M, 3-methylindole; I3PA, indole-3-pyruvic acid; I3SP, 3-indoxyl sulfate; I5OH, 5-hydroxyindole; I7OH, 7-hydroxyindole; IACN, 3-indolylacetonitrile; IMI, 1-methylindole; IND, indole; Kan, kanamycin; LB, Luria−Bertani; M9CA, minimal 9 casamino acid; PAS, Per-Arnt-Sim; PDB, protein database; RBS, ribosomal binding site; REC, receiver domain; RR, response regulator; TCS, two-component system.

■ REFERENCES

(1) Crook, N., Ferreiro, A., Gasparrini, A. J., Pesesky, M. W., Gibson, M. K., Wang, B., Sun, X., Condiotte, Z., Dobrowolski, S., Peterson, D., and Dantas, G. (2019) Adaptive strategies of the candidate probiotic *E. coli* Nissle in the mammalian gut. *Cell Host Microbe 25*, 499−512.

(2) Riglar, D. T., and Silver, P. A. (2018) Engineering bacteria for diagnostic and therapeutic applications. *Nat. Rev. Microbiol. 16*, 214−225.

(3) Daeffler, K. N., Galley, J. D., Sheth, R. U., Ortiz-Velez, L. C., Bibb, C. O., Shroyer, N. F., Britton, R. A., and Tabor, J. J. (2017) Engineering bacterial thiosulfate and tetrathionate sensors for detecting gut inflammation. *Mol. Syst. Biol. 13*, 923.

(4) Lee, J.-H., Wood, T. K., and Lee, J. (2015) Roles of indole as an interspecies and interkingdom signaling molecule. *Trends Microbiol. 23*, 707−718.

(5) Agus, A., Planchais, J., and Sokol, H. (2018) Gut microbiota regulation of tryptophan metabolism in health and disease. *Cell Host Microbe 23*, 716−724.

(6) Yano, J. M., Yu, K., Donaldson, G. P., Shastri, G. G., Ann, P., Ma, L., Nagler, C. R., Ismagilov, R. F., Mazmanian, S. K., and Hsiao, E. Y. (2015) Indigenous bacteria from the gut microbiota regulate host serotonin biosynthesis. *Cell 161*, 264−276.
(7) Clarke, G., McKernan, D. P., Gaszner, G., Quigley, E. M., Cryan, J. F., and Dinan, T. G. (2012) A distinct profile of tryptophan metabolism along the kynurenine pathway downstream of Toll-like receptor activation in irritable bowel syndrome. *Front. Pharmacol. 3*, 90.
(8) Zelante, T., Iannitti, R. G., Cunha, C., De Luca, A., Giovannini, G., Pieraccini, G., Zecchi, R., D'Angelo, C., Massi-Benedetti, C., Fallarino, F., Carvalho, A., Puccetti, P., and Romani, L. (2013) Tryptophan catabolites from microbiota engage aryl hydrocarbon receptor and balance mucosal reactivity *via* interleukin-22. *Immunity 39*, 372−385.
(9) Zelante, T., Puccetti, M., Giovagnoli, S., and Romani, L. (2021) Regulation of host physiology and immunity by microbial indole-3-aldehyde. *Curr. Opin. Immunol. 70*, 27−32.
(10) Scott, S. A., Fu, J., and Chang, P. V. (2020) Microbial tryptophan metabolites regulate gut barrier function *via* the aryl hydrocarbon receptor. *Proc. Natl. Acad. Sci. U. S. A. 117*, 19376−19387.
(11) Cervantes-Barragan, L., Chai, J. N., Tianero, M. D., Di Luccia, B., Ahern, P. P., Merriman, J., Cortez, V. S., Caparon, M. G., Donia, M. S., Gilfillan, S., Cella, M., Gordon, J. I., Hsieh, C. S., and Colonna, M. (2017) *Lactobacillus reuteri* induces gut intraepithelial CD4(+)-CD8alphaalpha(+) T cells. *Science 357*, 806−810.
(12) Yu, J., Luo, Y., Zhu, Z., Zhou, Y., Sun, L., Gao, J., Sun, J., Wang, G., Yao, X., and Li, W. (2019) A tryptophan metabolite of the skin microbiota attenuates inflammation in patients with atopic dermatitis through the aryl hydrocarbon receptor. *J. Allergy Clin. Immunol. 143*, 2108−2119.
(13) Rothhammer, V., Mascanfroni, I. D., Bunse, L., Takenaka, M. C., Kenison, J. E., Mayo, L., Chao, C. C., Patel, B., Yan, R., Blain, M., Alvarez, J. I., Kébir, H., Anandasabapathy, N., Izquierdo, G., Jung, S., Obholzer, N., Pochet, N., Clish, C. B., Prinz, M., Prat, A., Antel, J., and Quintana, F. J. (2016) Type I interferons and microbial metabolites of tryptophan modulate astrocyte activity and central nervous system inflammation *via* the aryl hydrocarbon receptor. *Nat. Med. 22*, 586−597.
(14) Powell, D. N., Swimm, A., Sonowal, R., Bretin, A., Gewirtz, A. T., Jones, R. M., and Kalman, D. (2020) Indoles from the commensal microbiota act *via* the AHR and IL-10 to tune the cellular composition of the colonic epithelium during aging. *Proc. Natl. Acad. Sci. U. S. A. 117*, 21519−21526.
(15) Bommarius, B., Anyanful, A., Izrayelit, Y., Bhatt, S., Cartwright, E., Wang, W., Swimm, A. I., Benian, G. M., Schroeder, F. C., and Kalman, D. (2013) A family of indoles regulate virulence and Shiga toxin production in pathogenic E. coli. *PLoS One 8*, e54456.
(16) Hicks, M., Bachmann, T. T., and Wang, B. (2020) Synthetic biology enables programmable cell-based biosensors. *ChemPhysChem 21*, 132−144.
(17) Naydich, A. D., Nangle, S. N., Bues, J. J., Trivedi, D., Nissar, N., Inniss, M. C., Niederhuber, M. J., Way, J. C., Silver, P. A., and Riglar, D. T. (2019) Synthetic gene circuits enable systems-level biosensor trigger discovery at the host-microbe interface. *mSystems 4*, e00125-19.
(18) Hubbard, T. D., Murray, I. A., Bisson, W. H., Lahoti, T. S., Gowda, K., Amin, S. G., Patterson, A. D., and Perdew, G. H. (2015) Adaptation of the human aryl hydrocarbon receptor to sense microbiota-derived indoles. *Sci. Rep. 5*, 12689.
(19) Hirakawa, H., Inazumi, Y., Masaki, T., Hirata, T., and Yamaguchi, A. (2005) Indole induces the expression of multidrug exporter genes in *Escherichia coli*. *Mol. Microbiol. 55*, 1113−1126.
(20) Boon, N., Kaur, M., Aziz, A., Bradnick, M., Shibayama, K., Eguchi, Y., and Lund, P. A. (2020) The signaling molecule indole inhibits induction of the AR2 acid resistance system in *Escherichia coli*. *Front. Microbiol. 11*, 474.
(21) Zarkan, A., Liu, J., Matuszewska, M., Gaimster, H., and Summers, D. K. (2020) Local and universal action: the paradoxes of indole signalling in bacteria. *Trends Microbiol. 28*, 566−577.
(22) Gaimster, H., Cama, J., Hernández-Ainsa, S., Keyser, U. F., and Summers, D. K. (2014) The indole pulse: a new perspective on indole signalling in Escherichia coli. *PLoS One 9*, e93168.
(23) Mann, T. H., Seth Childers, W., Blair, J. A., Eckart, M. R., and Shapiro, L. (2016) A cell cycle kinase with tandem sensory PAS domains integrates cell fate cues. *Nat. Commun. 7*, 11454.
(24) Porter, S. L., Wadhams, G. H., and Armitage, J. P. (2011) Signal processing in complex chemotaxis pathways. *Nat. Rev. Microbiol. 9*, 153−165.
(25) Henke, J. M., and Bassler, B. L. (2004) Three parallel quorum-sensing systems regulate gene expression in *Vibrio harveyi*. *J. Bacteriol. 186*, 6902−6914.
(26) Beier, D., and Gross, R. (2006) Regulation of bacterial virulence by two-component systems. *Curr. Opin. Microbiol. 9*, 143−152.
(27) Kowallis, K. A., Duvall, S. W., Zhao, W., and Childers, W. S. (2020) Manipulation of bacterial signaling using engineered histidine kinases, In *Histidine Phosphorylation*, pp 141−163, Springer.
(28) Krell, T., Lacal, J., Busch, A., Silva-Jimenez, H., Guazzaroni, M. E., and Ramos, J. L. (2010) Bacterial sensor kinases: diversity in the recognition of environmental signals. *Annu. Rev. Microbiol. 64*, 539−559.
(29) Schmidl, S. R., Sheth, R. U., Wu, A., and Tabor, J. J. (2014) Refactoring and optimization of light-switchable *Escherichia coli* two-component systems. *ACS Synth. Biol. 3*, 820−831.
(30) Ramakrishnan, P., and Tabor, J. J. (2016) Repurposing *Synechocystis* PCC6803 UirS−UirR as a UV-violet/green photoreversible transcriptional regulatory tool in *E. coli*. *ACS Synth. Biol. 5*, 733−740.
(31) Ong, N. T., Olson, E. J., and Tabor, J. J. (2018) Engineering an *E. coli* near-infrared light sensor. *ACS Synth. Biol. 7*, 240−248.
(32) Ong, N. T., and Tabor, J. J. (2018) A miniaturized *Escherichia coli* green light sensor with high dynamic range. *ChemBioChem 19*, 1255−1258.
(33) Olson, E. J., Hartsough, L. A., Landry, B. P., Shroff, R., and Tabor, J. J. (2014) Characterizing bacterial gene circuit dynamics with optically programmed gene expression signals. *Nat. Methods 11*, 449.
(34) Riglar, D. T., Giessen, T. W., Baym, M., Kerns, S. J., Niederhuber, M. J., Bronson, R. T., Kotula, J. W., Gerber, G. K., Way, J. C., and Silver, P. A. (2017) Engineered bacteria can function in the mammalian gut long-term as live diagnostics of inflammation. *Nat. Biotechnol. 35*, 653−658.
(35) Ganesh, I., Ravikumar, S., Yoo, I. K., and Hong, S. H. (2015) Construction of malate-sensing Escherichia coli by introduction of a novel chimeric two-component system. *Bioprocess Biosyst. Eng. 38*, 797−804.
(36) Ganesh, I., Ravikumar, S., Lee, S. H., Park, S. J., and Hong, S. H. (2013) Engineered fumarate sensing Escherichia coli based on novel chimeric two-component system. *J. Biotechnol. 168*, 560−566.
(37) Ravikumar, S., David, Y., Park, S. J., and Choi, J. I. (2018) A chimeric two-component regulatory system-based *Escherichia coli* biosensor engineered to detect glutamate. *Appl. Biochem. Biotechnol. 186*, 335−349.
(38) Selvamani, V., Ganesh, I., Maruthamuthu, M. K., Eom, G. T., and Hong, S. H. (2017) Engineering chimeric two-component system into *Escherichia coli* from *Paracoccus denitrificans* to sense methanol. *Biotechnol. Bioprocess Eng. 22*, 225−230.
(39) Teixeira, A. P., and Fussenegger, M. (2019) Engineering mammalian cells for disease diagnosis and treatment. *Curr. Opin. Biotechnol. 55*, 87−94.
(40) Schmidl, S. R., Ekness, F., Sofjan, K., Daeffler, K. N., Brink, K. R., Landry, B. P., Gerhardt, K. P., Dyulgyarov, N., Sheth, R. U., and Tabor, J. J. (2019) Rewiring bacterial two-component systems by modular DNA-binding domain swapping. *Nat. Chem. Biol. 15*, 690−698.
(41) Galperin, M. Y., Makarova, K. S., Wolf, Y. I., and Koonin, E. V. (2018) Phyletic distribution and lineage-specific domain architectures of archaeal two-component signal transduction systems. *J. Bacteriol.*, DOI: 10.1128/JB.00681-17.
(42) Levskaya, A., Chevalier, A. A., Tabor, J. J., Simpson, Z. B., Lavery, L. A., Levy, M., Davidson, E. A., Scouras, A., Ellington, A. D., Marcotte,

E. M., and Voigt, C. A. (2005) Synthetic biology: engineering *Escherichia coli* to see light. *Nature 438*, 441−442.
(43) Wang, B., Barahona, M., Buck, M., and Schumacher, J. (2013) Rewiring cell signalling through chimaeric regulatory protein engineering. *Biochem. Soc. Trans. 41*, 1195−1200.
(44) Papon, N., and Stock, A. M. (2019) Two-component systems. *Curr. Biol. 29*, R724−R725.
(45) Gao, R., and Stock, A. M. (2009) Biological insights from structures of two-component proteins. *Annu. Rev. Microbiol. 63*, 133−154.
(46) Gao, R., Mack, T. R., and Stock, A. M. (2007) Bacterial response regulators: versatile regulatory strategies from common domains. *Trends Biochem. Sci. 32*, 225−234.
(47) Whitaker, W. R., Davis, S. A., Arkin, A. P., and Dueber, J. E. (2012) Engineering robust control of two-component system phosphotransfer using modular scaffolds. *Proc. Natl. Acad. Sci. U. S. A. 109*, 18090.
(48) Francis, V. I., and Porter, S. L. (2019) Multikinase networks: two-component signaling networks integrating multiple stimuli. *Annu. Rev. Microbiol. 73*, 199−223.
(49) Park, D. M., and Taffet, M. J. (2019) Combinatorial sensor design in *Caulobacter crescentus* for selective environmental uranium detection. *ACS Synth. Biol. 8*, 807−817.
(50) Behnsen, J., and Raffatellu, M. (2013) Keeping the peace: aryl hydrocarbon receptor signaling modulates the mucosal microbiota. *Immunity 39*, 206−207.
(51) Osipiuk, J., Zhou, M., Freeman, L., and Joachimiak, A., and Midwest Center for Structural Genomics (MCSG). (2008) Crystal structure of PAS domain of HTR-like protein from *Haloarcula marismortui*. *Protein Data Bank*. https://www.rcsb.org/structure/3BWL. DOI: 10.2210/pdb3bwl/pdb.
(52) UniProt, C. (2019) UniProt: a worldwide hub of protein knowledge. *Nucleic Acids Res. 47*, D506−D515.
(53) Ohlendorf, R., Vidavski, R. R., Eldar, A., Moffat, K., and Moglich, A. (2012) From dusk till dawn: one-plasmid systems for light-regulated gene expression. *J. Mol. Biol. 416*, 534−542.
(54) Krueger, B., Friedrich, T., Förster, F., Bernhardt, J., Gross, R., and Dandekar, T. (2012) Different evolutionary modifications as a guide to rewire two-component systems. *Bioinf. Biol. Insights 6*, BBI.S9356.
(55) Moglich, A., Ayers, R. A., and Moffat, K. (2009) Design and signaling mechanism of light-regulated histidine kinases. *J. Mol. Biol. 385*, 1433−1444.
(56) Dubey, B. N., Lori, C., Ozaki, S., Fucile, G., Plaza-Menacho, I., Jenal, U., and Schirmer, T. (2016) Cyclic di-GMP mediates a histidine kinase/phosphatase switch by noncovalent domain cross-linking. *Science advances 2*, e1600823.
(57) Ptashne, M. (2004) *A Genetic Switch: Phage Lambda Revisited*, CSHL Press.
(58) Mutalik, V. K., Guimaraes, J. C., Cambray, G., Lam, C., Christoffersen, M. J., Mai, Q. A., Tran, A. B., Paull, M., Keasling, J. D., Arkin, A. P., and Endy, D. (2013) Precise and reliable gene expression *via* standard transcription and translation initiation elements. *Nat. Methods 10*, 354−360.
(59) Moglich, A., and Moffat, K. (2007) Structural basis for light-dependent signaling in the dimeric LOV domain of the photosensor YtvA. *J. Mol. Biol. 373*, 112−126.
(60) Engelhard, C., Diensthuber, R. P., Moglich, A., and Bittl, R. (2017) Blue-light reception through quaternary transitions. *Sci. Rep. 7*, 1385.
(61) Diensthuber, R. P., Bommer, M., Gleichmann, T., and Moglich, A. (2013) Full-length structure of a sensor histidine kinase pinpoints coaxial coiled coils as signal transducers and modulators. *Structure (Oxford, U. K.) 21*, 1127−1136.
(62) Duvall, S. W., and Childers, W. S. (2020) Design of a histidine kinase FRET sensor to detect complex signal integration within living bacteria. *ACS Sensors 5*, 1589−1596.
(63) Kowallis, K. A., Silfani, E. M., Kasumu, A. P., Rong, G., So, V., and Childers, W. S. (2020) Synthetic control of signal flow within a bacterial multi-kinase network. *ACS Synth. Biol. 9*, 1705−1713.
(64) Garbe, T. R., Kobayashi, M., and Yukawa, H. (2000) Indole-inducible proteins in bacteria suggest membrane and oxidant toxicity. *Arch. Microbiol. 173*, 78−82.
(65) Megaw, J., and Gilmore, B. F. (2017) Archaeal persisters: persister cell formation as a stress response in *Haloferax volcanii*. *Front. Microbiol.*, DOI: 10.3389/fmicb.2017.01589.
(66) Hendricks, M. R., Lashua, L. P., Fischer, D. K., Flitter, B. A., Eichinger, K. M., Durbin, J. E., Sarkar, S. N., Coyne, C. B., Empey, K. M., and Bomberger, J. M. (2016) Respiratory syncytial virus infection enhances *Pseudomonas aeruginosa* biofilm growth through dysregulation of nutritional immunity. *Proc. Natl. Acad. Sci. U. S. A. 113*, 1642−1647.
(67) Dong, F., Hao, F., Murray, I. A., Smith, P. B., Koo, I., Tindall, A. M., Kris-Etherton, P. M., Gowda, K., Amin, S. G., Patterson, A. D., and Perdew, G. H. (2020) Intestinal microbiota-derived tryptophan metabolites are predictive of Ah receptor activity. *Gut Microbes 12*, 1788899.
(68) Vyhlidalova, B., Krasulova, K., Pecinkova, P., Marcalikova, A., Vrzal, R., Zemankova, L., Vanco, J., Travnicek, Z., Vondracek, J., Karasova, M., Mani, S., and Dvorak, Z. (2020) Gut microbial catabolites of tryptophan are ligands and agonists of the aryl hydrocarbon receptor: a detailed characterization. *Int. J. Mol. Sci. 21*, 2614.
(69) Moglich, A., Ayers, R. A., and Moffat, K. (2009) Structure and signaling mechanism of Per-ARNT-Sim domains. *Structure 17*, 1282−1294.
(70) Leyser, O. (2018) Auxin Signaling. *Plant Physiol. 176*, 465−479.
(71) Spaepen, S., and Vanderleyden, J. (2011) Auxin and plant-microbe interactions. *Cold Spring Harbor Perspect. Biol. 3*, a001438.
(72) Remans, R., Ramaekers, L., Schelkens, S., Hernandez, G., Garcia, A., Reyes, J. L., Mendez, N., Toscano, V., Mulling, M., Galvez, L., and Vanderleyden, J. (2008) Effect of Rhizobium−Azospirillum coinoculation on nitrogen fixation and yield of two contrasting Phaseolus vulgaris L. genotypes cultivated across different environments in Cuba. *Plant Soil 312*, 25−37.
(73) Bashan, Y., and Holguin, G. (1997) Azospirillum − plant relationships: environmental and physiological advances (1990−1996). *Can. J. Microbiol. 43*, 103−121.
(74) Navarro, L., Dunoyer, P., Jay, F., Arnold, B., Dharmasiri, N., Estelle, M., Voinnet, O., and Jones, J. D. G. (2006) A Plant miRNA Contributes to Antibacterial Resistance by Repressing Auxin Signaling. *Science (Washington, DC, U. S.) 312*, 436.
(75) Lee, J., Attila, C., Cirillo, S. L., Cirillo, J. D., and Wood, T. K. (2009) Indole and 7-hydroxyindole diminish Pseudomonas aeruginosa virulence. *Microb. Biotechnol. 2*, 75−90.
(76) Hillson, N. J., Rosengarten, R. D., and Keasling, J. D. (2012) j5 DNA assembly design automation software. *ACS Synth. Biol. 1*, 14−21.
(77) Gibson, D. G., Young, L., Chuang, R.-Y., Venter, J. C., Hutchison, C. A., and Smith, H. O. (2009) Enzymatic assembly of DNA molecules up to several hundred kilobases. *Nat. Methods 6*, 343−345.
(78) Ittiamornkul, K., Zhu, Q., Gkotsi, D. S., Smith, D. R. M., Hillwig, M. L., Nightingale, N., Goss, R. J. M., and Liu, X. (2015) Promiscuous indolyl vinyl isonitrile synthases in the biogenesis and diversification of hapalindole-type alkaloids. *Chem. Sci. 6*, 6836−6840.
(79) Slabinski, L., Jaroszewski, L., Rychlewski, L., Wilson, I. A., Lesley, S. A., and Godzik, A. (2007) XtalPred: a web server for prediction of protein crystallizability. *Bioinformatics 23*, 3403−3405.
(80) Altschul, S. F., Gish, W., Miller, W., Myers, E. W., and Lipman, D. J. (1990) Basic local alignment search tool. *J. Mol. Biol. 215*, 403−410.
(81) Waterhouse, A. M., Procter, J. B., Martin, D. M., Clamp, M., and Barton, G. J. (2009) Jalview Version 2 - a multiple sequence alignment editor and analysis workbench. *Bioinformatics 25*, 1189−1191.
(82) Crooks, G. E., Hon, G., Chandonia, J. M., and Brenner, S. E. (2004) WebLogo: a sequence logo generator. *Genome Res. 14*, 1188−1190.
(83) Schneider, T. D., and Stephens, R. M. (1990) Sequence logos: a new way to display consensus sequences. *Nucleic Acids Res. 18*, 6097−6100.

https://doi.org/10.1021/acssynbio.1c00090
ACS Synth. Biol. 2021, 10, 1605−1614